

Complex-Scaling Calculation of Three-Body Resonances Using Complex-Range Gaussian Basis Functions

— Application to 3α resonances in ^{12}C —

Shin-Ichi OHTSUBO¹, Yoshihiro FUKUSHIMA¹, Masayasu KAMIMURA²
and Emiko HIYAMA²

¹*Department of Applied Physics, Fukuoka University, Fukuoka 814-0180, Japan*
²*RIKEN Nishina Center, RIKEN, Wako 351-0198, Japan*

We propose to use the complex-range Gaussian basis functions, $\{r^l e^{-(1\pm i\omega)(r/r_n)^2} Y_{lm}(\hat{\mathbf{r}}); r_n \text{ in a geometric progression}\}$, in the calculation of three-body resonances with the complex-scaling method (CSM) in which use is often made of the real-range Gaussian basis functions, $\{r^l e^{-(r/r_n)^2} Y_{lm}(\hat{\mathbf{r}})\}$, that are suitable for describing the short-distance structure and the asymptotic decaying behavior of few-body systems. The former basis set is more powerful than the latter when describing the resonant and nonresonant continuum states with highly oscillating amplitude at large scaling angles θ . We applied the new basis functions to the CSM calculation of the 3α resonances with $J = 0^+, 2^+$ and 4^+ in ^{12}C . The eigenvalue distribution of the complex scaled Hamiltonian becomes more precise and the maximum scaling angle becomes drastically larger ($\theta_{\max} = 16^\circ \rightarrow 36^\circ$) than those given by the use of the real-range Gaussians. Owing to these advantages, we were able to confirm the prediction by Kurokawa and Katō [Phys. Rev. C **71**, 021301 (2005)] on the appearance of the new broad 0_3^+ state; we show it as an explicit resonance pole isolated from the 3α continuum.

§1. Introduction

The complex scaling method (CSM)^{1),2),3),4),5)} is a very powerful tool to investigate resonances in quantum many-body systems. Application of the CSM to the nuclear physics problems are extensively reviewed in Ref. 6) and references therein. In the CSM the resonance parameters can be obtained by using only L^2 (bound state type) wave functions and without the explicit scattering calculations or without the use of the continuum wave functions; namely, the energy E_r and the decay width Γ of a resonance can be obtained by solving the eigenvalue problem for the complex scaled Schrödinger equation with a scaling angle θ , $[H(\theta) - E(\theta)]\Psi(\theta) = 0$, where $\Psi(\theta)$ are expanded in terms of only L^2 integrable many-body basis functions.

In the CSM, there is a limitation of the scaling angle θ due to the analyticity of the Hamiltonian. Furthermore, in practical calculations, one often meets a difficulty in solving resonant states with large decay width since the complex scaled Hamiltonian is diagonalized with a limited number of basis functions. A set of real-range Gaussians, $\{r^l e^{-(r/r_n)^2} Y_{lm}(\hat{\mathbf{r}}); r_n \text{ in a geometric progression}\}$,^{7),8),9),10)} are often employed as the basis functions. But, it is difficult for the basis set to describe highly oscillating wave functions that appears in the CSM when the scaling angle becomes large; the overlap matrix of the basis set becomes easily ill-conditioned when the number of basis functions is rather large.

Thus, one of the purposes of the present work is to propose the use of the complex-range Gaussian basis functions, $\{r^l e^{-(1\pm i\omega)(r/r_n)^2} Y_{lm}(\hat{\mathbf{r}})\}$,^{9),10)} in the CSM calculation of three-body resonances so as to overcome the above difficulty for the large θ . Owing to the oscillating component, the space of the new function set becomes much larger and the overlap matrix hardly becomes ill-conditioned. This improves the quality of the CSM calculation significantly and increases the possible scaling angle drastically.

One of the most intensively studied nuclei using the three-body CSM is ^{12}C nucleus as the 3α -cluster system. The CSM has especially been useful to investigate the 3α resonance structure in its excited states. Such CSM studies of ^{12}C are reviewed in Refs. 11) and 12) and references therein. Among the studies, Kurokawa and Katō^{11),12)} succeeded in thoroughly calculating the energies and decay widths of the 3α resonant states in ^{12}C with the total angular momentum $J = 0$ to 5.

In Table I, it is interesting to see the recently accomplished reasonable agreement between the results by the calculation^{11),12)} and the observation¹³⁾ on the 0_3^+ , 0_4^+ and 2_2^+ states. Especially, Kurokawa-Katō's prediction of the new 0_3^+ state having a large width is of importance to understand the new experimental

Table I. New results of the recent calculation^(11),12) and experiment⁽¹³⁾ on the 0_3^+ , 0_4^+ and 2_2^+ states in ^{12}C . The excitation energies (E_x) and decay widths (Γ) are given in MeV. See also the footnote below.

^{12}C	CAL ^(11),12)		EXP ⁽¹³⁾	
	E_x	Γ	E_x	Γ
0_3^+	8.95	1.48	9.04 ± 0.09	1.45 ± 0.18
0_4^+	11.87	1.1	10.56 ± 0.06	1.42 ± 0.08
2_2^+	9.57	1.1	9.84 ± 0.06	1.01 ± 0.15

results in Ref. 13).*) Their CSM calculation was performed at the scaling angle of 16° that is the largest angle available in the calculation using the real-range Gaussian basis. Since the angle is not enough for separating the low-lying broad 0_3^+ resonance from the continuum eigenvalues, they made an extrapolation by applying the method of analytic continuation of the coupling constant (ACCC)^(14),15) combined with the CSM (ACCC+CSM)⁽¹⁶⁾ in order to derive the complex energy of the 0_3^+ resonance. But, Arai⁽¹⁷⁾ reported that, the 0_3^+ resonance obtained in Ref. 11) is missing from his calculation based on the microscopic R -matrix method for the $^8\text{Be}(0^+, 2^+, 4^+) + \alpha$ two-body scattering problem. However, in the calculation in Ref. 17), the ^8Be was described with the bound-state approximation employing only four different tempered Gaussian functions for the α - α relative motion.

Thus, the second purpose of the present paper is to apply the CSM with the complex-range Gaussian basis functions to the 3α resonances in ^{12}C and examine the results in Refs. 11) and 12). Since the function space of the present basis set is very large, we have the following advantages: i) the distribution of the eigenvalues of the complex scaled Hamiltonian becomes much more precise than those obtained in the literature, and ii) the scaling angle is drastically increased from $\theta = 16^\circ$ up to 36° that is enough large to separate explicitly the 0_3^+ resonance pole from the 3α continuum eigenvalues.

The present paper is organized as follows: in Section 2, we introduce the complex-range Gaussian basis functions and incorporate them into the framework of CSM. In Section 3, we apply the method to the 3α resonances in ^{12}C and compare the result with that obtained in Refs. 11) and 12). Summary is given in Section 4.

§2. Method

2.1. Three-body complex scaling method

In many cases of the CSM studies, the three-body wave function is expanded in terms of the real-range Gaussian basis set with ranges in a geometric progression. In this work, we propose to use the complex-range Gaussians in the three-body CSM calculations.

We explain it, as an example, taking the case of $^{12}\text{C}(= \alpha + \alpha + \alpha)$ on the basis of the orthogonality condition model (OCM)⁽¹⁸⁾ for the 3α system. The extension from the real-range Gaussian to the complex-range ones in other three-body systems is straightforward. We take all the three sets of Jacobi coordinates (Fig. 1), $\mathbf{r}_1 = \mathbf{x}_2 - \mathbf{x}_3$ and $\mathbf{R}_1 = \mathbf{x}_1 - \frac{1}{2}(\mathbf{x}_2 + \mathbf{x}_3)$ and cyclically for $(\mathbf{r}_2, \mathbf{R}_2)$ and $(\mathbf{r}_3, \mathbf{R}_3)$, \mathbf{x}_i being the position vector of i th particle.

The Hamiltonian is written as

$$H = \sum_{i=1}^3 t_i - T_G + \sum_{i=1}^3 V_{\alpha\alpha}(r_i) + V_{3\alpha}(r_1, r_2, r_3) + V_{\text{Pauli}}. \quad (2.1)$$

The operators t_i and T_G stand for the kinetic energies of i th α particle and the center of mass motion, respectively. $V_{\alpha\alpha}$ is the α - α potential and V_{Pauli} is a pseudo potential representing the Pauli principle

*) As for the 0^+ data in Fig. 8(a) in Ref. 13), we employ the interpretation by the authors that there are two 0^+ resonance peaks as summarized in Table I and that the resonances may correspond respectively to the 0_3^+ and 0_4^+ states described in Ref. 11). The authors showed another interpretation to regard the peaks as a single peak at $E_x = 9.93 \pm 0.03$ MeV with a width of 2.71 ± 0.08 MeV.

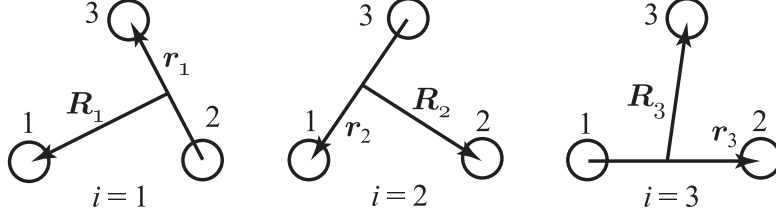


Fig. 1. Three sets of the Jacobi coordinates for three α particles.

between α clusters. The 3α potential $V_{3\alpha}$ is introduced if necessary. These potentials are explained in Subsection 3.1.

In the CSM, the radial coordinates are transformed by

$$r_i \rightarrow r_i e^{i\theta}, \quad R_i \rightarrow R_i e^{i\theta}. \quad (2.2)$$

The transformed Hamiltonian is denoted by $H(\theta)$. We solve the equation

$$[H(\theta) - E(\theta)]\Psi(\theta) = 0 \quad (2.3)$$

by expanding $\Psi(\theta)$ in terms of the totally symmetric L^2 -integrable three-body basis functions $\{\Psi_\gamma; \gamma = 1, \dots, \gamma_{\max}\}$:

$$\Psi(\theta) = \sum_{\gamma=1}^{\gamma_{\max}} C_\gamma(\theta) \Psi_\gamma. \quad (2.4)$$

The complex eigenenergies and the expansion coefficients are determined by

$$\sum_{\gamma'=1}^{\gamma_{\max}} [H_{\gamma\gamma'}(\theta) - E(\theta)N_{\gamma\gamma'}] C_{\gamma'}(\theta) = 0 \quad (\gamma = 1, \dots, \gamma_{\max}), \quad (2.5)$$

where the overlap and Hamiltonian matrix elements are respectively written as

$$N_{\gamma\gamma'} = \langle \Psi_\gamma | \Psi_{\gamma'} \rangle, \quad (2.6)$$

and

$$H_{\gamma\gamma'}(\theta) = \langle \Psi_\gamma | H(\theta) | \Psi_{\gamma'} \rangle. \quad (2.7)$$

The complex resonance energy is given, independently of θ in principle, by

$$E_{res} = E_r - \frac{i\Gamma}{2}, \quad (2.8)$$

where E_r is the resonance energy with respect to the 3α breakup threshold and Γ is the total decay width.

The symmetric three-body basis functions Ψ_γ in (2.4) is written as

$$\Psi_\gamma = \Phi_\gamma(\mathbf{r}_1, \mathbf{R}_1) + \Phi_\gamma(\mathbf{r}_2, \mathbf{R}_2) + \Phi_\gamma(\mathbf{r}_3, \mathbf{R}_3). \quad (2.9)$$

We express each $\Phi_\gamma(\mathbf{r}_i, \mathbf{R}_i)$ as a product of a function of \mathbf{r}_i and that of \mathbf{R}_i :

$$\Phi_\gamma(\mathbf{r}_i, \mathbf{R}_i) = \phi_{nl}(r_i) \psi_{NL}(R_i) \left[Y_l(\hat{\mathbf{r}}_i) Y_L(\hat{\mathbf{R}}_i) \right]_{JM}, \quad (2.10)$$

where γ specifies a set of quantum numbers

$$\gamma \equiv \{nl, NL, JM\}. \quad (2.11)$$

J is the total angular momentum and M is its z -component.

2.2. Real-range Gaussian basis functions

According to the Gaussian expansion method (GEM),^{7),8),9),10)} we take the radial shape of $\phi_{nl}(r)$ and $\psi_{NL}(r)$ in (2.10) as follows:

$$\phi_{nl}(r) = r^l e^{-(r/r_n)^2}, \quad (2.12)$$

$$\psi_{NL}(R) = R^L e^{-(R/R_N)^2}, \quad (2.13)$$

where normalization constants are omitted for simplicity. The GEM recommends to set the Gaussian ranges in a geometric progression:

$$r_n = r_1 a^{n-1} \quad (n = 1, \dots, n_{\max}), \quad (2.14)$$

$$R_N = R_1 A^{N-1} \quad (N = 1, \dots, N_{\max}). \quad (2.15)$$

This greatly reduces the nonlinear parameters to be optimized. We designate a set of the geometric sequence by $\{n_{\max}, r_1, r_{n_{\max}}\}$ instead of $\{n_{\max}, r_1, a\}$ and similarly for $\{N_{\max}, R_1, R_{N_{\max}}\}$, which is more convenient for consideration of the spatial distribution of the basis set.

The basis set $\{\phi_{nl}; n = 1, \dots, n_{\max}\}$ has the following properties: i) They range from very compact to very diffuse, more densely in the inner region than in the outer one. While the basis functions with small ranges are responsible for describing the short-range structure of the system, the basis with longest-range parameters is for the asymptotic behavior. ii) After multiplication by normalization constants for $\langle \phi_{nl} | \phi_{nl} \rangle = 1$, they have the relation

$$\langle \phi_{nl} | \phi_{n+kl} \rangle = \left(\frac{2a^k}{1+a^{2k}} \right)^{l+3/2}, \quad (2.16)$$

which shows that the overlap with the k th neighbor is *independent* of n , decreasing gradually with increasing k . We thus expect that the coupling among all the basis functions takes place smoothly and coherently so as to describe properly both the short-range structure and long-range decaying behavior simultaneously.

We note that a single Gaussian $e^{-(r/r_n)^2}$ decays quickly as r increases, but appropriate superposition of many Gaussians can decay even exponentially with increasing r up to a sufficiently large r . Good examples are shown in Figs. 3 and 4 in Ref. 9).

2.3. Complex-range Gaussian basis functions

For the precise CSM calculations of three-body systems, however, we improve the Gaussian shape to have more sophisticated (but still tractable) radial dependence. This is because that the wave function in CSM becomes more oscillatory as the scaling angle θ increases. But, the superposition of the real-range Gaussians is difficult to accurately describe oscillatory functions having several nodes.

In the GEM in Ref. 9), it was proposed to improve the Gaussian shape by introducing the *complex* range instead of the real one:

$$\phi_{nl}^{(+\omega)}(r) = r^l e^{-(1+i\omega)(r/r_n)^2}, \quad (2.17)$$

$$\phi_{nl}^{(-\omega)}(r) = r^l e^{-(1-i\omega)(r/r_n)^2}, \quad (2.18)$$

and

$$\psi_{NL}^{(+\omega)}(R) = R^L e^{-(1+i\omega)(R/R_N)^2}, \quad (2.19)$$

$$\psi_{NL}^{(-\omega)}(R) = R^L e^{-(1-i\omega)(R/R_N)^2}, \quad (2.20)$$

where the ranges r_n and R_N are given by (2.14) and (2.15), respectively. Using the above complex conjugate pairs, $\phi_{nl}^{(\pm\omega)}(r)$ and $\psi_{NL}^{(\pm\omega)}(R)$, we can construct equivalent sets of *real* basis functions:

$$\phi_{nl}^{(\cos)}(r) = r^l e^{-(r/r_n)^2} \cos \omega(r/r_n)^2, \quad (2.21)$$

$$\phi_{nl}^{(\sin)}(r) = r^l e^{-(r/r_n)^2} \sin \omega(r/r_n)^2, \quad (2.22)$$

and

$$\psi_{NL}^{(\cos)}(R) = R^L e^{-(R/R_N)^2} \cos \omega(R/R_N)^2, \quad (2.23)$$

$$\psi_{NL}^{(\sin)}(R) = R^L e^{-(R/R_N)^2} \sin \omega(R/R_N)^2. \quad (2.24)$$

In the present CSM calculation of ^{12}C , the former set, (2.17)-(2.20), is employed^{*)} and the three-body basis function $\Phi_\gamma(\mathbf{r}_i, \mathbf{R}_i)$ of (2.10) is replaced by

$$\Phi_\gamma(\mathbf{r}_i, \mathbf{R}_i) = \phi_{nl}^{(\pm\omega)}(r) \psi_{NL}^{(\pm\omega)}(R_i) \left[Y_l(\hat{\mathbf{r}}_i) Y_L(\hat{\mathbf{R}}_i) \right]_{JM}, \quad (2.25)$$

with γ specifying a set

$$\gamma \equiv \{\pm\omega, nl; \pm\omega, NL; JM\}, \quad (2.26)$$

where one can take different ω 's between $\phi(r)$ and $\psi(R)$ although it was not necessary in the present 3α CSM calculation.

The new basis functions, (2.17)-(2.24), apparently extend the function space from the old ones, (2.12) and (2.13), since they have the oscillating components; their applications are seen in Refs. 9), 19), 20), 21), 22), 10). Note that the computation programming is almost the same as that for (2.12) and (2.13) although some of real variables are changed to complex ones.

In order to compare visually the real-range and complex-range Gaussians, we plot, in Fig. 2, $\phi_{nl}(r)$ of (2.12), $\phi_{nl}^{(\cos)}(r)$ of (2.21) and $\phi_{nl}^{(\sin)}(r)$ of (2.22) with $l = 0$, $r_n = 5$ fm and $\omega = 1.0$ and $\pi/2$. A good test of the use of complex-range Gaussians is to calculate the wave functions of highly excited states in a three-dimensional harmonic oscillator (HO) potential. We calculate the $l = 0$ neutron wave function in the potential with $\hbar\omega = 15.0$ MeV. The wave function, Ψ_l , is expanded in terms of totally 32 basis functions of (2.21) and (2.22) as

$$\Psi_l(r) = \sum_{n=1}^{n_{\max}} \left[c_{nl}^{(\cos)} \phi_{nl}^{(\cos)}(r) + c_{nl}^{(\sin)} \phi_{nl}^{(\sin)}(r) \right] \quad (2.27)$$

with $n_{\max} = \frac{32}{2}$ and $\omega = 1$, and in terms of 32 real-range Gaussians (2.12) as

$$\Psi_l(r) = \sum_{n=1}^{n_{\max}} c_{nl} \phi_{nl}(r) \quad (2.28)$$

with $n_{\max} = 32$. The expansion coefficients and the eigenenergies are obtained by diagonalizing the Hamiltonian in the space. Optimized nonlinear parameters of the complex-range Gaussian set are $\{n_{\max} = \frac{32}{2}, r_1 = 1.4$ fm, $r_{n_{\max}} = 7.1$ fm, $\omega = 1.0\}$ and those for the real-range Gaussians are $\{n_{\max} = 32, r_1 = 0.6$ fm, $r_{n_{\max}} = 16.0$ fm $\}$. The range parameters are given by round numbers, but further optimization does not give any significant change to the result.

In Table II, the calculated energies (in the number of quanta) are compared with the exact ones. The result with the complex-range Gaussians is much better than that with the real-range Gaussians especially in the highly oscillatory states as is expected. It is to be noted that the both cases have the same number of basis functions and that the overlap matrix of the real-range Gaussian basis set becomes heavily ill-conditioned when the range parameters $\{r_1, r_{n_{\max}}\}$ are taken to be the same as those of the complex-range Gaussian set. Extension of the function space due to making the range parameters complex is much more effective than the simple extension having two times more functions in the real-range Gaussian set.

In Fig. 3, wave function of the 36-quanta state obtained with the complex-range Gaussians is compared with the exact one. The two curves for those wave functions overlap to each other everywhere; the difference is less than 0.001 in the unit of the vertical axis.

We thus expect that use of the new basis set (2.17)-(2.20) in three-body CSM calculations well describes the highly oscillating wave functions of both the resonant and nonresonant continuum states even when the scaling angle becomes rather large.

^{*)} We made the same calculation employing the latter set, (2.21)-(2.24) to crosscheck the computation programs and obtained, as a matter of course, the same result.

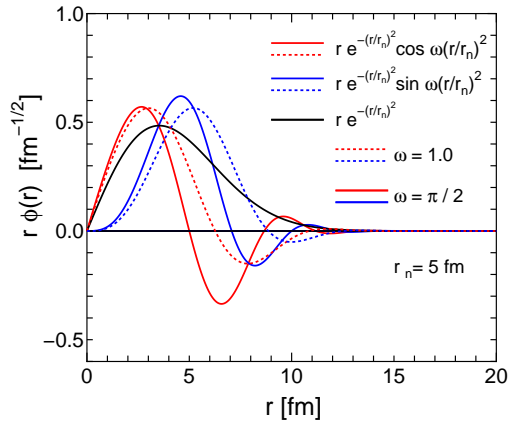


Fig. 2. An example of the $l = 0$ complex-range Gaussian basis functions presented in the form of Eqs. (2.21) and (2.22) with $r_n = 5$ fm and $\omega = 1.0$ and $\pi/2$. The functions are normalized to unity.

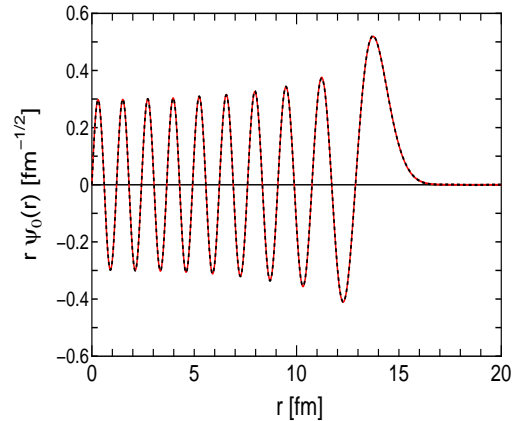


Fig. 3. Wave function of the $l = 0$ 36-quanta state for the HO potential using 32 complex-range Gaussians (black dotted line). Deviation from the exact one (red solid line) is everywhere less than 0.001 in the unit of the vertical axis.

Table II. Energies (number of quanta) of the highly excited $l=0$ states of the HO potential calculated using 32 complex-range Gaussians with $\{n_{\max}=\frac{32}{2}, r_1=1.4$ fm, $r_{n_{\max}} = 7.1$ fm, $\omega = 1.0\}$ and 32 real-range Gaussians with $\{n_{\max}=32, r_1=0.6$ fm, $r_{n_{\max}} = 16.0$ fm $\}$.

Exact	Complex-range Gaussians	real-range Gaussians
0	10^{-13}	10^{-14}
12	12.000000003	12.00003
16	16.000000005	16.003
20	20.00000005	20.1
24	24.0000004	24.6
28	28.00002	30.1
32	32.0003	36.8
36	36.0004	45.2
40	40.04	56.7
44	44.2	71.7

§3. Application to 3α resonances in ^{12}C

3.1. Interaction of the 3α system

We take the same model and interaction as those in Refs. 11) and 12). The potential $V_{\alpha\alpha}$ is constructed by folding the effective N - N interaction by Schmid-Wildermuth²³⁾ and the Coulomb potential into the density of the α cluster having the $(0s)^4$ configuration. In Refs. 11) and 12), the $V_{\alpha\alpha}$ is adjusted to reproduce the experimental phase shift of the α - α system by taking $1.03 \times V_{\alpha\alpha}$.

The Pauli principle between α clusters is taken into account by the OCM.¹⁸⁾ The OCM projection operator,²⁴⁾ V_{Pauli} , in the Hamiltonian (2.1) is written by

$$V_{\text{Pauli}} = \lim_{\lambda \rightarrow \infty} \lambda \sum_f |f\rangle \langle f|, \quad (3.1)$$

which rules out the Pauli-forbidden α - α relative states ($f = 0S, 1S, 0D$) from the three-body wave function. In this work, we take $\lambda = 10^5$ MeV.

Since use of the 2α potential $V_{\alpha\alpha}$ together with the Pauli potential V_{Pauli} makes the energies of the ground-rotational-band states ($0_1^+, 2_1^+, 4_1^+$) lower than the observed values, the repulsive 3α potential $V_{3\alpha}$ in (2.1) is introduced in Refs. 11) and 12) phenomenologically in the form

$$V_{3\alpha}(r_1, r_2, r_3) = V_{3\alpha}^{J\pi} \exp[-\mu(r_1^2 + r_2^2 + r_3^2)], \quad \mu = 0.15 \text{ fm}^{-2}, \quad (3.2)$$

where $V_{3\alpha}^{0+} = 31.7$ MeV, $V_{3\alpha}^{2+} = 63.0$ MeV and $V_{3\alpha}^{4+} = 150.0$ MeV are employed dependently on the total angular momentum $J = 0^+, 2^+$ and 4^+ , respectively.

3.2. The 0^+ resonances

Figure 4, taken from Ref. 11), shows the 0^+ eigenvalue distribution of the complex scaled Hamiltonian calculated with the real-range Gaussian basis functions. The scaling angle $\theta = 16^\circ$ was the maximum angle available in the calculation. The new broad 0_3^+ state was predicted at $E_{res} = 1.66 - i 0.74$ MeV, but this complex energy is not isolated from the $[\alpha + \alpha + \alpha] + [{}^8\text{Be}(0^+) + \alpha]$ continuum states in Fig. 4 at $\theta = 16^\circ$. The energy was derived by an extrapolation based on the ACCC+CSM (see Fig. 2 in Ref. 11)).

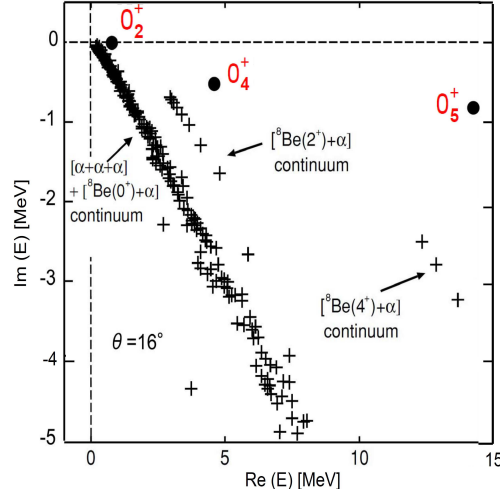


Fig. 4. The 0^+ eigenvalue distribution of the complex scaled Hamiltonian for the 3α system obtained by Kurokawa and Katō⁽¹¹⁾ using the real-range Gaussian basis functions. The scaling angle is $\theta = 16^\circ$. The 0_3^+ state was predicted at $E_{res} = 1.66 - i 0.74$ MeV, not localized from the $[\alpha + \alpha + \alpha] + [{}^8\text{Be}(0^+) + \alpha]$ continuum (see the text). This figure is taken from Ref.⁽¹¹⁾

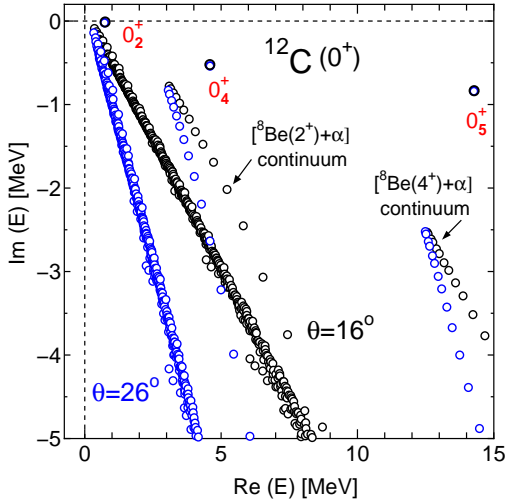


Fig. 5. The 0^+ eigenvalue distribution of the complex scaled Hamiltonian for the 3α system with the use of the complex-range Gaussian basis set in Table III. The scaling angles are $\theta = 16^\circ$ (black) and 26° (blue). This figure is to be compared with Fig. 4.

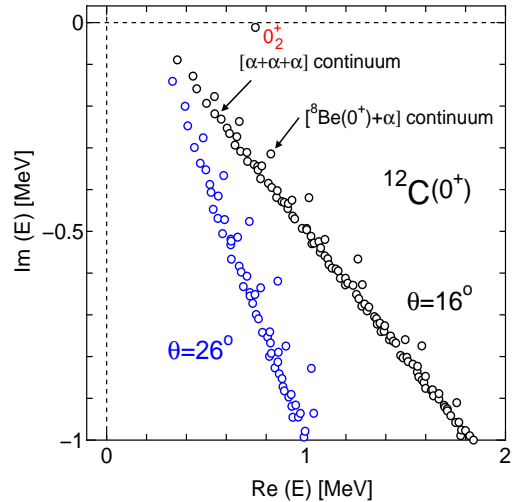


Fig. 6. The low-energy part of Fig. 5 is enlarged to show that the $[{}^8\text{Be}(0^+) + \alpha]$ continuum is distinguishable from the $[\alpha + \alpha + \alpha]$ one by ~ 0.1 MeV which corresponds to the energy of ${}^8\text{Be}(0^+)$ measured from the α - α threshold.

Figure 5 illustrates the result of the present CSM calculation for the $J = 0^+$ states at $\theta = 16^\circ$ and 26° . The low-energy part is enlarged in Fig. 6. All the nonlinear parameters used in the calculation are listed in Table III. The parameters for the Gaussian ranges are given in round numbers but further optimization of them does not significantly improve the present result; the same is for the ranges of the

Table III. All the nonlinear parameters of the $J = 0^+$ three-body complex-range Gaussian basis functions for ^{12}C used in the CSM calculation of Fig. 5 at $\theta = 16^\circ$ and 26° . Total number of the basis is $\gamma_{\max} = 3200$ with $\omega = \pi/2$.

$J = 0^+$		$r^l e^{-(1\pm i\omega)(r/r_n)^2}$		$R^l e^{-(1\pm i\omega)(R/R_N)^2}$				$\omega = \pi/2$
l	n_{\max}	r_1 [fm]	$r_{n_{\max}}$ [fm]	L	N_{\max}	R_1 [fm]	$R_{N_{\max}}$ [fm]	number of basis
0	16	0.3	30.0	0	16	0.5	40.0	1024
2	16	0.6	30.0	2	16	1.0	40.0	1024
4	18	1.0	30.0	4	16	1.5	40.0	1152

$J = 2^+$ and 4^+ states. The slightly larger basis set for $l = L = 4$ is necessary to precisely generate the $[\text{}^8\text{Be}(4^+) + \alpha]$ continuum.

The $[\alpha + \alpha + \alpha]$ continuum for $\theta = 16^\circ$ is much less scattered than that in Fig. 4 and the $[\text{}^8\text{Be}(0^+) + \alpha]$ continuum is distinguishable in Fig. 6 from the former continuum by ~ 0.1 MeV which corresponds to the energy of the $\text{}^8\text{Be}(0^+)$ resonance measured from the α - α threshold. It is to be emphasized that, in Fig. 5, the localized resonance poles of the 0_2^+ , 0_4^+ and 0_5^+ states for $\theta = 26^\circ$ remain at the same places of them for $\theta = 16^\circ$ and that the complex energies of the three-body continuum still form a narrow straight band with little scattered members. The energies and widths of those resonances are almost the same as those obtained in Ref. 11).

3.3. The new 0_3^+ resonance

In order to investigate the new 0_3^+ state that was predicted by Kurokawa and Katō,^{(11), (12)} we performed the CSM calculation for the scaling angles from $\theta = 22^\circ$ up to 36° . These large angles are required to reveal explicitly such a low-lying broad resonance separated from the $[\alpha + \alpha + \alpha] + [\text{}^8\text{Be}(0^+) + \alpha]$ continuum states. The employed set of the three-body complex-range Gaussian basis functions is listed in Table IV. Such a larger number of the basis is necessary for this purpose.

Table IV. All the nonlinear parameters of the $J = 0^+$ three-body complex-range Gaussian basis functions for ^{12}C used in the CSM calculation of Fig. 7 for $\theta = 22^\circ$ to 36° to reveal the 0_3^+ resonance state. Total number of basis is $\gamma_{\max} = 4448$ with $\omega = \pi/2$.

$J = 0^+$		$r^l e^{-(1\pm i\omega)(r/r_n)^2}$		$R^l e^{-(1\pm i\omega)(R/R_N)^2}$				$\omega = \pi/2$
l	n_{\max}	r_1 [fm]	$r_{n_{\max}}$ [fm]	L	N_{\max}	R_1 [fm]	$R_{N_{\max}}$ [fm]	number of basis
0	22	0.3	40.0	0	22	0.5	40.0	1936
2	22	0.6	40.0	2	22	1.0	40.0	1936
4	12	1.0	30.0	4	12	1.5	30.0	576

In Fig. 7, we illustrate the 0^+ distribution of complex eigenvalues for $\theta = 22^\circ$ up to 36° . Only for $\theta = 36^\circ$ both the $[\alpha + \alpha + \alpha]$ continuum (open blue boxes) and the $[\text{}^8\text{Be}(0^+) + \alpha]$ continuum (open blue circles) are given, but the former is omitted for $\theta < 36^\circ$ to avoid complexity of the figure. We observe a converged resonance pole at $E_{res} = 0.79 - i0.84$ MeV (the closed blue circle) and identify it as the third 0^+ state that was predicted in Ref. 11). The position and width of the resonance, however, differ slightly from the result in Ref. 11), $E_{res} = 1.66 - i0.74$ MeV.

Reason of this difference is explained with Fig. 8 which is to be compared with Fig. 2 in Ref. 11). Figure 8 illustrates the trajectory of the 0_3^+ state on the complex energy plane, that was obtained by changing the strength parameter δ of the auxiliary three-body potential, Eq. (4) in Ref. 11), added to the Hamiltonian (2.1),

$$V_{\text{aux.}} = \delta \exp[-\mu(r_1^2 + r_2^2 + r_3^2)], \quad \mu = 0.15 \text{ fm}^{-2}. \quad (3.3)$$

The closed blue circle for $\delta = 0$ in Fig. 8 is the same as that for the 0_3^+ resonance in Fig. 7. On the other hand, in Ref. 11), the direct CSM calculation of the 0_3^+ resonance was not possible when the auxiliary 3α

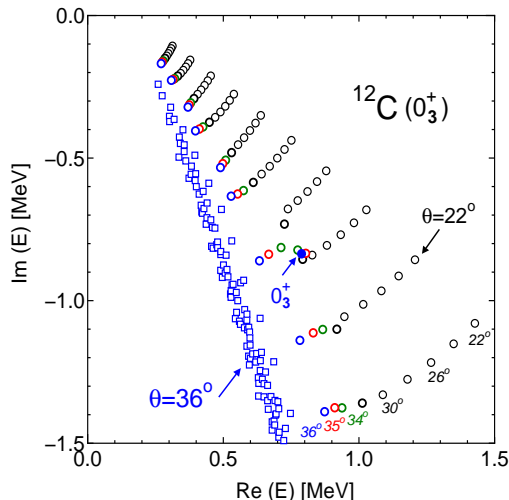


Fig. 7. The 0^+ eigenvalue distribution of the complex scaled Hamiltonian in which the angle θ is varied from 22° to 36° . The 0_3^+ resonance appears, as the closed blue circle (36°), at $E_{res} = 0.79 - i0.84$ MeV. Only for $\theta = 36^\circ$ both the continua of $[\alpha + \alpha + \alpha]$ (open blue boxes) and $[{}^8\text{Be}(0^+) + \alpha]$ (open blue circles) are given, but the former is omitted for $\theta < 36^\circ$ for clarity of the figure.

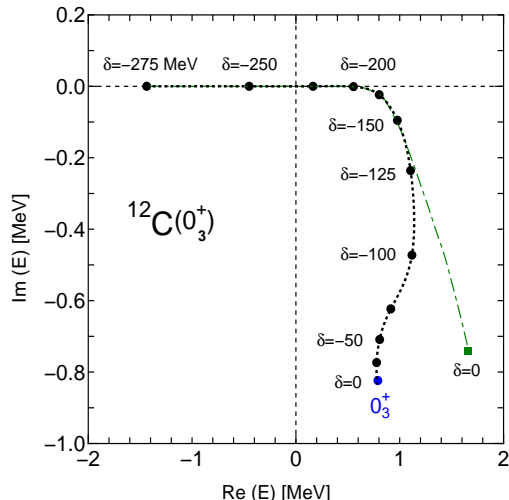


Fig. 8. Trajectory of the 0_3^+ state obtained by changing the strength parameter δ of the auxiliary three-body potential (3.3). The blue closed circle at $\delta = 0$ corresponds to the 0_3^+ resonance in Fig. 7. The green box denotes the 0_3^+ state predicted by Kurokawa and Katō^{(11), (12)} on the basis of the extrapolation (the dash-dotted green curve, taken from Ref. 11) using the ACCC+CSM.

potential is less attractive than $\delta = -120$ MeV. The green box that indicates the 0_3^+ state in Ref. 11) was therefore estimated by the extrapolation (the dash-dotted green curve) using the ACCC+CSM. We thus understand that the difference in the resonance-pole position between the two calculations comes from the error of the extrapolation.

We conclude that we have confirmed the prediction by Kurokawa and Katō⁽¹¹⁾ about the appearance of a new 0_3^+ broad resonance that is located slightly above the Hoyle state (0_2^+). As long as the structure of the 0_3^+ state is concerned, it is interesting to see that, in Fig. 7, the converged pole of the state is generated from the $[{}^8\text{Be}(0^+) + \alpha]$ continuum during the scaling angle is rotated up to $\theta = 36^\circ$. Therefore, the 0_3^+ state is considered to be dominantly composed of the $[{}^8\text{Be}(0^+) + \alpha]$ configuration. Kurokawa and Katō⁽¹²⁾ pointed out that the 0_3^+ state has a similar property to the 0_2^+ state and the former may be a higher nodal state of the latter having the $[{}^8\text{Be}(0^+) + 0^+(\alpha)]$ configuration mainly, which is consistent with our conjecture.

Table V. All the nonlinear parameters of the $J = 2^+$ three-body complex-range Gaussian basis functions for ${}^{12}\text{C}$ used in the CSM calculation of Fig. 9 at $\theta = 16^\circ$ and 26° . Total number of the basis is $\gamma_{\max} = 6400$ with $\omega = \pi/2$.

$J = 2^+$		$r^l e^{-(1 \pm i\omega)(r/r_n)^2}$		$R^l e^{-(1 \pm i\omega)(R/R_N)^2}$				$\omega = \pi/2$
l	n_{\max}	r_1 [fm]	$r_{n_{\max}}$ [fm]	L	N_{\max}	R_1 [fm]	$R_{N_{\max}}$ [fm]	number of basis
0	16	0.3	30.0	2	16	1.0	40.0	1024
2	16	0.6	30.0	0	16	0.5	40.0	1024
2	16	0.6	30.0	2	16	1.0	40.0	1024
2	16	0.6	30.0	4	16	1.5	40.0	1024
4	18	1.0	30.0	2	16	1.0	40.0	1152
4	18	1.0	30.0	4	16	1.5	40.0	1152

3.4. The 2^+ resonances

Figure 9 illustrates the calculated 2^+ eigenvalue distribution of the complex scaled Hamiltonian for the 3α system. The scaling angles are $\theta = 16^\circ$ and 26° . This figure is much more precise than Fig. 5

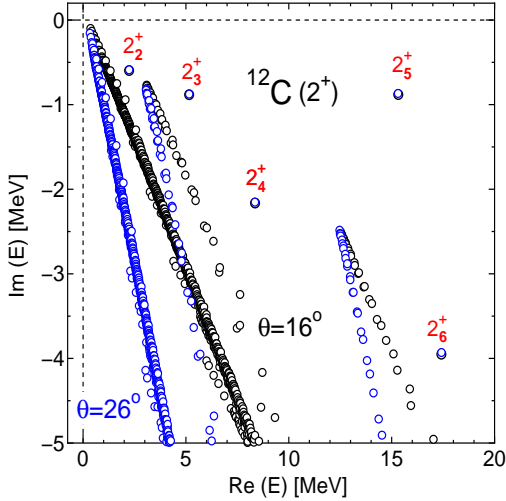


Fig. 9. The 2^+ eigenvalue distribution of the complex scaled Hamiltonian calculated with the complex-range Gaussian basis set in Table V. The scaling angles are $\theta = 16^\circ$ (black) and 26° (blue). This figure is to be compared with Fig. 5 in Ref. 12) at $\theta = 16^\circ$.

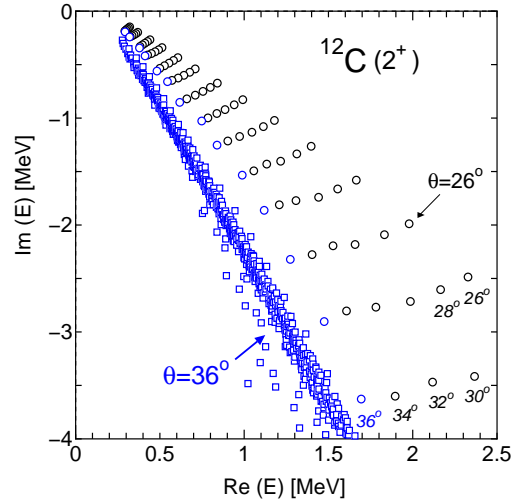


Fig. 10. Low-energy part of the 2^+ eigenvalue distribution for $\theta = 26^\circ$ to 36° . Any 2^+ resonance, like the 0_3^+ state in Fig. 7, does not appear in the upper-right side of the $[\alpha + \alpha + \alpha]$ continuum (blue boxes) at $\theta = 36^\circ$. See also the caption of Fig. 7.

($\theta = 16^\circ$) in Ref. 12) for the 2^+ eigenvalue distribution. All the nonlinear parameters used for calculating Fig. 9 are listed in Table V. Total number of the basis is $\gamma_{\max} = 6400$ with $\omega = \pi/2$.

Calculated five resonances denoted as $2_2^+, \dots, 2_6^+$ appear at almost the same complex energies of those obtained in Ref. 12). We observe no other 2^+ resonance at low energies. As shown in Fig. 10, even if the scaling angle is increased up to $\theta = 36^\circ$, any new 2^+ resonance, like the 0_3^+ resonance in Fig. 7, does not appear in the upper-right side of the $[\alpha + \alpha + \alpha]$ continuum at $\theta = 36^\circ$.

3.5. The 4^+ resonances

The calculated 4^+ eigenvalue distribution of the complex scaled Hamiltonian is illustrated in Fig. 11. The resonance parameters are summarized in Table VI together with the result by Kurokawa and Katō.¹²⁾ All the nonlinear parameters of the basis set are listed in Table VII. We note that the lowest 4^+ resonance at $E_{res} = 4.96 - i 1.1$ MeV in Fig. 11 is missing in Ref. 12), where the lowest one is given at $E_{res} = 6.82 - i 0.12$

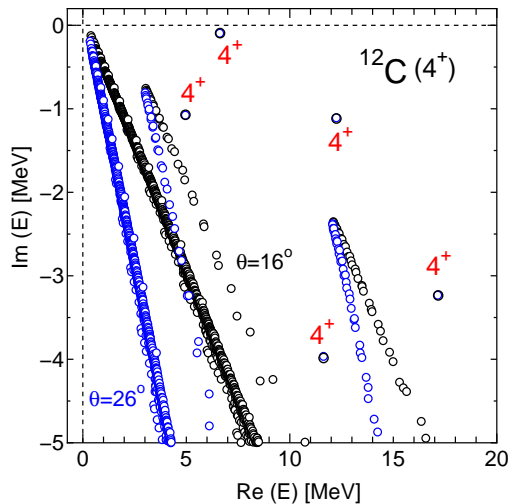


Fig. 11. The 4^+ eigenvalue distribution of the complex scaled Hamiltonian for the 3α system calculated with the complex-range Gaussian basis set in Table VII. The scaling angles are $\theta = 16^\circ$ (black) and 26° (blue). The lowest resonance at $E_{res} = 4.96 - i 1.1$ MeV does not correspond to the observed 4_1^+ state at $E_r = 6.81$ MeV which is reproduced by the second 4^+ resonance in this figure. See the text about this problem.

Table VI. Calculated resonance parameters for the $J = 4^+$ states in ^{12}C by the present work and Ref. 12) which employ the same interaction. All quantities are given in MeV.

^{12}C	present work			Ref. 12)			
	J^π	E_x	E_r	Γ	E_x	E_r	Γ
	4^+	12.25	4.96	2.2	—	—	—
	4^+	13.91	6.61	0.20	14.11	6.82	0.24
	4^+	18.92	11.62	8.0	—	—	—
	4^+	19.53	12.23	2.2	20.39	13.1	3.4
	4^+	24.41	17.11	6.3	—	—	—

Table VII. All the nonlinear parameters of the $J = 4^+$ three-body complex-range Gaussian basis functions for ^{12}C used in the CSM calculation of Fig. 11 at $\theta = 16^\circ$ and 26° . Total number of the basis is $\gamma_{\text{max}} = 8640$ with $\omega = \pi/2$.

$J = 4^+$		$r^l e^{-(1\pm i\omega)(r/r_n)^2}$		$R^l e^{-(1\pm i\omega)(R/R_N)^2}$				$\omega = \pi/2$
l	n_{max}	r_1 [fm]	$r_{n_{\text{max}}}$ [fm]	L	N_{max}	R_1 [fm]	$R_{N_{\text{max}}}$ [fm]	number of basis
0	20	0.3	30.0	4	18	1.0	40.0	1440
2	20	0.6	30.0	2	18	0.5	40.0	1440
2	20	0.6	30.0	4	18	1.0	40.0	1440
4	20	0.6	30.0	0	18	1.5	40.0	1440
4	20	1.0	30.0	2	18	1.0	40.0	1440
4	20	1.0	30.0	4	18	1.5	40.0	1440

MeV, but it corresponds to the second 4^+ state in Fig. 11.

This situation causes a serious problem in the determination of the 3α potential $V_{3\alpha}$ of Eq. (3.2). The strongly repulsive factor of $V_{3\alpha}^{4^+} = 150.0$ MeV was so chosen in Ref. 12) that the calculated lowest 4^+ state can reproduce the observed value of $E_{res}(4_1^+) = 6.808 - i0.258$ MeV. However, by the introduction of the repulsive 3α potential, the original lowest 4^+ state at -1.66 MeV (with $V_{3\alpha}^{4^+} = 0$) is pushed up to $E_{res} = 6.61 - i0.10$ MeV which corresponds to the observed 4_1^+ state, but the second 4^+ state (with $V_{3\alpha}^{4^+} = 0$) remains almost unaffected at $E_{res}(4^+) = 4.96 - i1.1$ MeV that becomes the lowest 4^+ state in Fig. 11.

Therefore, we understand that the introduction of the 3α potential $V_{3\alpha}$ does not work for the $J = 4^+$ states even if the strength is given dependently on J . Any appropriate determination of the interaction in the 3α system will be required in future 3α OCM-CSM calculations.

§4. Summary

The authors have proposed to use the complex-range Gaussian basis functions, $\{r^l e^{-(1\pm i\omega)(r/r_n)^2} Y_{lm}(\hat{\mathbf{r}}); r_n \text{ in a geometric progression}\}$, in the CSM calculations of three-body resonances in place of the real-range Gaussians that are often employed in the literature. The former-type Gaussians are very suitable for describing short-range correlations, long-range asymptotic decaying amplitudes and highly oscillating behavior in few-body systems as well as they are tractable in calculating the Hamiltonian matrix elements with transformation between different sets of Jacobi coordinates.⁹⁾ Therefore, they are particularly useful in the CSM calculations when representing the resonant and nonresonant continuum states that become quite oscillatory as the scaling angle θ increases; this enables us, in the study of broad three-body resonances, to take much larger angles than those considered before and to have a possibility of observing new broad resonance poles.

The present method has been applied to the 3α resonances in ^{12}C with $J = 0^+, 2^+$ and 4^+ . The result was compared with that obtained by Kurokawa and Katō^{(11), (12)} where the real-range Gaussians were employed to expand the 3α wave function. In Table VIII, we summarize the calculated energies

Table VIII. Summary of the calculated result for the $J = 0^+$ and 2^+ in ^{12}C by the present work together with the result by Refs. 11) and 12) and the experimental data. The data for $E_x = 9.04, 9.84$ and 10.56 MeV are taken from Ref. 13); see the footnote in Section 1. The other data are taken from Ref. 25). The model and interaction are the same between the two calculations. All quantities are given in MeV.

^{12}C	present work			Refs. 11) and 12)			Experimental data			
	J^π	E_x	E_r	Γ	E_x	E_r	Γ	E_x	E_r	Γ
0_1^+	0.00	-7.30	—	0.00	-7.29	—	0.00000	-7.2747	—	—
2_1^+	4.32	-2.98	—	4.31	-2.98	—	4.43891	-2.8358	—	—
0_2^+	8.05	0.75	0.0088	8.05	0.76	0.0024	7.65420	0.3795	8.5×10^{-6}	—
0_3^+	8.09	0.79	1.68	8.95	1.66	1.48	9.04(9)	1.77	1.45(18)	—
2_2^+	9.54	2.24	1.2	9.57	2.28	1.1	9.84(6)	2.57	1.01(15)	—
0_4^+	11.89	4.59	1.0	11.87	4.58	1.1	10.56(6)	3.29	1.42(8)	—
2_3^+	12.47	5.15	1.8	12.43	5.14	1.9	11.16(5)	3.89	0.43(8)	—
2_4^+	15.67	8.36	4.3	15.93	8.64	3.9	15.44(4)	8.17	1.5(2)	—
0_5^+	21.60	14.3	1.7	21.59	14.3	1.5	—	—	—	—
2_5^+	22.70	15.3	1.8	22.39	15.1	1.2	—	—	—	—
2_6^+	24.70	17.4	8.0	24.89	17.6	6.0	—	—	—	—

and widths of the states with $J = 0^+$ and 2^+ together with the result by Refs. 11) and 12) and the experimental data. The result for the 4^+ resonances, having a problem in the interaction employed, was summarized in Table VI.

The distribution of eigenvalues of the complex scaled Hamiltonian at $\theta = 16^\circ$ and 26° were found to become very precise (Figs. 5, 6, 9 and 11). The prediction of the new broad 0_3^+ resonance by Kurokawa and Katō¹¹⁾ was confirmed by our calculation; namely, as the scaling angle θ increases up to 36° , the 0_3^+ resonance pole becomes clearly separated from the $[\alpha + \alpha + \alpha]$ and $[^8\text{Be}(0^+) + \alpha]$ continuum states (Fig. 7). The slight deviation of the 0_3^+ resonance energy E_r by 0.9 MeV in Ref. 11) from our result is attributed to the error of the extrapolation¹¹⁾ of the resonance position by the ACCC+CSM (Fig. 8). As for the $0_4^+, 0_5^+, 2_2^+, 2_3^+, 2_4^+, 2_5^+$ and 2_6^+ resonances, we obtained almost the same energies and widths as those in Refs. 11) and 12). We did not observe any 2^+ low-lying broad resonance, like the 0_3^+ , as long as we increased the scaling angle θ up to 36° (Fig. 10).

We employed the same interaction for the 3α system as used in Refs. 11) and 12), but the calculation did not satisfactorily well reproduce the observed energy of the important Hoyle state (0_2^+), $E_r = 0.38$ MeV, with a deviation of some 0.4 MeV higher. Furthermore, the strongly repulsive 3α potential for the $J = 4^+$ states, introduced in Ref. 12) to reproduce the observed energy of the 4_1^+ state, is found to be not appropriate because the lowest 4^+ state in the present work is the broad resonance at $E_{res} = 4.96 - i 1.1$ MeV (Fig. 11) which was missing in Ref. 12) and the second 4^+ state corresponds to the observed 4_1^+ state.

We explicitly listed, in small tables, all the nonlinear parameters of the basis functions used in the present calculation of ^{12}C ($0^+, 2^+, 4^+$); our method is so transparent. For the comprehensive understanding of the 3α cluster structure of ^{12}C , however, use of more improved interactions is highly desirable in future studies.

Acknowledgements

The authors would like to thank Professor K. Katō for valuable discussion on the complex scaling method and the 3α -cluster structure of ^{12}C . Thanks are also due to Dr. T. Matsumoto for helpful discussions on the numerical complex scaling calculations. The authors thank the Yukawa Institute for Theoretical Physics at Kyoto University. Discussions during the YITP workshop YITP-W-12-19 on “Resonances and non-Hermitian systems in quantum mechanics” were useful to complete this work. The numerical calculations were performed on the HITACHI SR16000 at KEK, at Research Institute for Information Technology, Kyushu University and at Yukawa Institute for Theoretical Physics, Kyoto University.

References

- 1) J. Aguilar and J.M. Combes, *Commun. Math. Phys.* **22**, 269 (1971).
- 2) E. Balslev and J.M. Combes, *Commun. Math. Phys.* **22**, 280 (1971).
- 3) B. Simon, *Commun. Math. Phys.* **27**, 1 (1972).
- 4) Y.K. Ho, *Phys. Rep.* **99**, 1 (1983).
- 5) N. Moiseyev, *Phys. Rep.* **302**, 212 (1998).
- 6) S. Aoyama, T. Myo, K. Katō, and K. Ikeda, *Prog. Theor. Phys.* **116**, 1 (2006).
- 7) M. Kamimura, *Phys. Rev. A* **38**, 621 (1988).
- 8) H. Kameyama, M. Kamimura, and Y. Fukushima, *Phys. Rev. C* **40**, 974 (1989).
- 9) E. Hiyama, Y. Kino, and M. Kamimura, *Prog. Part. Nucl. Phys.* **51**, 223 (2003).
- 10) E. Hiyama, *Prog. Theor. Exp. Phys.* (2012) 01A204.
- 11) C. Kurokawa and K. Katō, *Phys. Rev. C* **71**, 021301 (R) (2005).
- 12) C. Kurokawa and K. Katō, *Nucl. Phys. A* **792**, 82 (2007).
- 13) M. Itoh, H. Akimune, M. Fujiwara, U. Garg, N. Hashimoto, T. Kawabata, K. Kawase, S. Kishi, T. Murakami, K. Nakanishi, Y. Nakatsugawa, B. K. Nayak, S. Okumura, H. Sakaguchi, H. Takeda, S. Terashima, M. Uchida, Y. Yasuda, M. Yosoi, and J. Zenihiro, *Phys. Rev. C* **84**, 054308 (2011).
- 14) V.I. Kukulin and V.M. Krasnopol'sky, *J. Phys. A* **10** L33 (1977); V.I. Kukulin, V.M. Krasnopol'sky, and M. Miselkhi, *Sov. J. Nucl. Phys.* **29**, 421 (1979).
- 15) V.I. Kukulin, V.M. Krasnopol'sky, and J. Horáček, *Theory of resonances: Principles and Applications*, (Kluwer Academic Publishers, Dordrecht, Netherlands, 1989), p. 219.
- 16) S. Aoyama, *Phys. Rev. C* **68**, 034313 (2003).
- 17) K. Arai, *Phys. Rev. C* **74** (2006) 064311.
- 18) S. Saito, *Prog. Theor. Phys.* **40**, 893 (1968); **41**, 705 (1969); *Prog. Theor. Phys.(Suppl.)* **62**, 11 (1977).
- 19) T. Matsumoto, T. Kamizato, K. Ogata, Y. Iseri, E. Hiyama, M. Kamimura, and M. Yahiro, *Phys. Rev. C* **68**, 064607 (2003).
- 20) H. Nakada, K. Mizuyama, M. Yamagami, and M. Matsuo, *Nucl. Phys. A* **828**, 283 (2009).
- 21) M. Kamimura, E. Hiyama, and Y. Kino, *Prog. Theor. Phys.* **121**, 1059 (2009).
- 22) E. Hiyama and M. Kamimura, *Phys. Rev. A* **85**, 022502 (2012); *Phys. Rev. A* **85**, 062505 (2012).
- 23) E.W. Schmit and K. Wildermuth, *Nucl. Phys.* **26**, 463 (1961).
- 24) V.I. Kukulin, V.M. Krasnopol'sky, V.T. Voronchev, and P. B. Sazonov, *Nucl. Phys. A* **417**, 128 (1984).
- 25) F. Ajzenberg-Selobe, *Nucl. Phys. A* **506**, 1 (1990).